ARTICLE TYPE

Cite this: DOI: 00.0000/xxxxxxxxxx

Highly air-stable, n-doped conjugated polymers achieved by dimeric organometallic dopants

Yu Yamashita*[a,b], Samik Jhulki[c], Dinesh Bhardwaj[c,d], Elena Longhi[c], Shohei Kumagai[a], Shun Watanabe[a,e], Stephen Barlow*[c], Seth R. Marder*[c], Jun Takeya[a,b]

Received Date
Accepted Date

DOI: 00.0000/xxxxxxxxxx

Chemical doping is a key process for controlling the electronic properties of molecular semiconductors, including their conductivity and work function. A common limitation of n-doped polymers is their instability under ambient conditions, which has imposed restrictions on the characterisation and device application of n-doped polymers. In this study, sequential n-doping with organometallic dopants was performed on thin films of polymeric semiconductors with naphthalene diimide and perylene diimide-based backbones. Moderate ambient stability was achieved with $(RuCp^*Mes)_2$, {Cp* = pentamethylcyclopentadienyl; Mes = 1,3,5-trimethylbenzene}, which is in striking contrast to the unstable, n-doped state obtained with cobaltocene, a simple one-electron reductant. The highly cathodic, effective redox potential of $(RuCp^*Mes)_2$, ca. −2.0 V vs ferrocene, suppresses the back electron transfer reaction and subsequent dopant loss in air, which gives rise to the observed air stability. It also allows a perylene diimide-based polymer to be reduced to state in which the repeat units are largely dianionic. Photoelectron measurements show that the ionization potential of the heavily doped polymer is ca. 3.9 eV. Our findings show that chemical doping with $(RuCp^*Mes)_2$ is an effective method to produce highly stable, n-doped conjugated polymers.

Introduction

π-Conjugated molecular materials capable of efficient charge transport are desirable for the development of opto-electronic devices through solution-based techniques. The charge-transport ability of these materials can be enhanced by molecular doping that introduces charge carriers through electron transfer reactions with molecular oxidants and reductants [1,2]. Recent studies have demonstrated that heavily p-doped (n-doped) polymeric semiconductors show a notably high (low) work function upon doping, which form an Ohmic contact when used as an injection layer [3–5]. These factors motivate the study of doped semiconductors to achieve high doping levels and concomitant charge transport properties [6,7].

In a conventional solution-doping process, dopant and semiconductor molecules are mixed in solution (Scheme 1**a**), which is then cast on substrates by drop-casting, spin-coating, or other solution-based techniques. Limitations of this method may include poor solubility of the doped systems and uncontrolled aggregation of the semiconductor and dopant molecules, which can limit the attainable doping efficiency and electrical properties. Some of these limitations can be overcome by employing a more recently developed 'sequential doping' technique. In this technique, a thin film of polymeric semiconductor is fabricated, which is then exposed to dopant vapour or solution (scheme 1**b**, **c**) [6,7]. When an

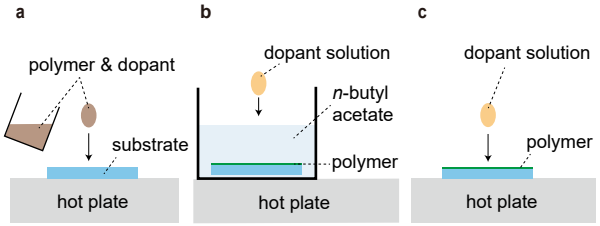

Scheme 1. (a) Mixed-solution doping. Sequential doping by (b) immersion method and (c) drop-casting method.

[a] *Material Innovation Research Center and Department of Advanced Material Science, Graduate School of Frontier Sciences, The University of Tokyo, Kashiwa, Chiba, Japan.*
[b] *International Center for Materials Nanoarchitectonics (MANA), National Institute for Materials Science, Tsukuba, Ibaraki, Japan.*
[c] *School of Chemistry and Biochemistry and Center for Organic Photonics and Electronics, Georgia Institute of Technology, Atlanta, U.S.A.*
[d] *CSIR-National Physical Laboratory, New Delhi, Delhi, India.*
[e] *PRESTO, JST, Kawaguchi, Saitama, Japan.*
† Electronic Supplementary Information (ESI) available:
See DOI: 00.0000/00000000.

effective combination of the semiconductor and dopant is used, intercalation of the guest dopant into the host polymer occurs, which leads to a high doping level throughout the thin film.[7–9].

Electronic devices such as photovoltaics and organic light-emitting diodes, which make use of an electron-transporting layer, can benefit from n-doping to enhance electron extraction/injection and transport[3,10]. Naphthalene diimide (NDI) and perylene diimide (PDI) are representative π-conjugated units that show good electron-transporting behavior[11–13]. P(NDI2OD-T2) (Figure 1a), a NDI-containing polymer, has been widely studied in devices such as field-effect transistors and photovoltaic cells[12,14]. Doping of P(NDI2OD-T2) with a suitable reducing agent results in conductivities of 10^{-1}–10^{-5} S cm^{-1} in an inert atmosphere[15,16]. A common difficulty in employing n-doped polymeric semiconductors in optoelectronic devices is that many of these materials are sensitive to ambient air, which necessitates their processing and handling in an inert atmosphere[1]. For this reason, recent research efforts have focused on achieving ambient-stable n-doping through the development of novel dopants and polymers[17–19]. However, the role of different dopants in imparting stability to doped films from a given polymer is not yet clear.

As an organometallic dopant, cobaltocene ($CoCp_2$, Cp = cyclopentadienyl) is a strong reducing agent, which is highly reactive and degrades rapidly upon exposure to ambient air[20] due to reaction with oxygen and/or water. The stability of strongly reducing organometallic dopants has been increased by developing dimeric dopants such as $(RhCp_2)_2$ and $(RuCp^*Mes)_2$, {Cp* = pentamethylcyclopentadienyl; Mes = 1,3,5-trimethylbenzene} (Figure 1a). A few minutes of exposure to ambient air before their use does not cause any discernible decomposition[21,22]. However, little is known about the stability of polymer thin films containing such dopants.

Here, we report the sequential doping of P(NDI2OD-T2)[12] and a PDI-based polymer, P(PDI-EB)[23] (Figure 2a), with $CoCp_2$ and $(RuCp^*Mes)_2$[21,22,24] (Figure 1a) to evaluate their electrical properties and stability. Intriguingly, $(RuCp^*Mes)_2$-doped P(PDI-EB) exhibits moderate air stability, despite an ionization potential of 3.9 eV. In addition, the UV-Vis and vibrational spectroscopy results suggest that P(PDI-EB) is approaching the dianion state by $(RuCp^*Mes)_2$ doping. The differences in the ambient stability of $CoCp_2$- and $(RuCp^*Mes)_2$-doped films are discussed based on the chemical equilibrium of the charge-transfer reactions.

Results and discussion

Sequential doping was conducted by exposing P(NDI2OD-T2) thin films to dopant solutions containing $CoCp_2$ or $(RuCp^*Mes)_2$. The thin films were first prepared on 1 cm^2 glass substrates by spin-coating of pristine polymer solution in chloroform followed by thermal annealing at 200 °C. In the case of chemical doping through the immersion method (Scheme 1b), the pristine thin-film samples were immersed in 1 mL *n*-butyl acetate (*n*BA) inside a glass vial, with the sample facing upwards. While heating the system at 80 °C, 30–40 μL of 2 mM solution of dopant in *n*BA was added to the vial. After one min, the thin-film samples were removed from the vial and dried at 80 °C prior to characterisation. An alternate method is drop-casting of a 2 mM dopant solution in *n*BA onto the thin films at 80 °C (Scheme 1c). All of the thin-film fabrications and doping processes were conducted in an Ar atmosphere.

Figure 1b shows the UV-Vis spectra of the P(NDI2OD-T2) thin films before and after doping with $CoCp_2$ measured in air. The $CoCp_2$-doped sample without encapsulation shows features corresponding to the undoped state. We observed that the $CoCp_2$-doped film without encapsulation changed its colour after air exposure at a time scale of 1 min, which was ascribed to the dedoping. To obtain the UV-Vis spectrum of the doped state, encapsulation was conducted after $CoCp_2$ doping in an Ar atmosphere, where the top surface of the doped film was covered with a CYTOP polymer and an additional glass substrate (see the Methods section). The spectrum of the encapsulated sample was consistent with previous reports of n-doped P(NDI2OD-T2)[26].

The time scale of the dedoping process was dramatically prolonged when $(RuCp^*Mes)_2$ was employed as the dopant for a P(NDI2OD-T2) thin film. Here, the P(NDI2OD-T2) thin films were doped with $(RuCp^*Mes)_2$ using the immersion method. The UV-

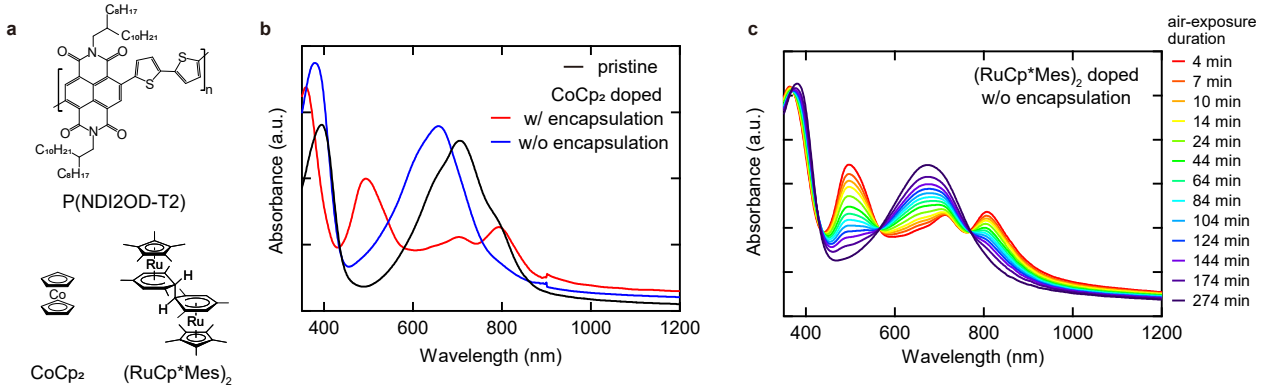

Figure 1 (a) Chemical structures of P(NDI2OD-T2), $CoCp_2$, and $(RuCp^*Mes)_2$. (b) UV-Vis spectra of the P(NDI2OD-T2) thin film before and after $CoCp_2$ doping via the drop-casting method. (c) UV-Vis absorption spectra of P(NDI2OD-T2) doped with $(RuCp^*Mes)_2$ through the immersion method. Spectra were measured repeatedly in air without encapsulation. The graph legends show the air-exposure time.

Vis spectra were measured in air without encapsulation with time (Figure 1c). The spectrum obtained after air exposure was consistent with that of the doped state of P(NDI2OD-T2). The spectra obtained in air over time indicated that most of the dedoping process occurred within approximately 200 min, which is two orders of magnitude longer than in the case of $CoCp_2$ doping.

The dedoped films showed very similar absorption spectra to that of a pristine film for the both $CoCp_2$ and $(RuCp^*Mes)_2$ doping, which suggests that the dedoping process involves a charge-transfer reaction and no significant changes in the chemical structure of the polymer occur. Interestingly, thermal annealing of the dedoped films resulted in the recovery of the doped states (Supplementary Figure S1†) in the $(RuCp^*Mes)_2$-doped samples, which further indicates that the dedoping process does not alter the chemical structure of the polymer. For a charge-transfer reaction that does not cause chemical degradation, the chemical equilibrium is a key factor for understanding the doping and dedoping kinetics. When the redox potentials of the dopant and semiconductor are comparable, as in the case of the semiconductors examined here and $CoCp_2$ (ca. -1.3 V vs. $FeCp_2^+/FeCp_2$), both forward and reverse electron-transfer processes may occur. The back electron transfer process is endergonic by only ca. 0.3 eV, implying that some fraction of the dopant is in the neutral state at all times. Given that neutral $CoCp_2$ is known to degrade in air[20], the neutral fraction of $CoCp_2$ in a doped film undergoes decomposition, which would drive the equilibrium, ultimately leading to rapid dedoping of the thin film. This hypothesis is consistent with the reported air stability of $CoCp_2^+$ salts formed with redox-inactive anions (e.g., PF_6^-) and with less-easily oxidised anions (e.g., the radical anion of tetracyanoquinodimethane, TCNQ)[20,27], where $CoCp_2$ is expected to remain in the cation state.

In the case of doping with $(RuCp^*Mes)_2$, air-stable 18-electron $RuCp^*Mes^+$ is produced, with a reduction potential of ca. -2.7 V vs. $FeCp_2^+/FeCp_2$[28]; thus, the back electron transfer from the doped polymer is a considerably endergonic reaction. This essentially eliminates back electron transfer from the doped polymer to $RuCp^*Mes^+$ followed by the degradation of the neutral dopant species as a dedoping pathway.

Another expected dedoping process is direct oxidation of a n-doped polymer to a neutral compound by oxygen in air[10]. Redox reactions between a n-doped polymer and oxygen in air would occur for $CoCp_2$- and $(RuCp^*Mes)_2$-doped polymers in a similar manner. Thus, very fast dedoping only in $CoCp_2$ doped polymers is likely due to the dedoping process through back electron transfer discussed above, which proceeds only for $CoCp_2$ doped polymers.

When the drop-casting method was employed with $(RuCp^*Mes)_2$ to P(NDI2OD-T2), doping proceeded further (Supplementary Figure S2†) to achieve a more heavily doped state, similarly to a spectroelectrochemical study[26]. Note that observation of this heavily doped state of P(NDI2OD-T2) through UV-vis measurements required encapsulation of the thin film owing to the instability of this state. Two-fold changes upon chemical doping with $(RuCp^*Mes)_2$ were also examined for a P(PDI-EB) thin film, where the observed moderate air stability allowed for a detailed analysis. Peaks at 632 and 728 nm were

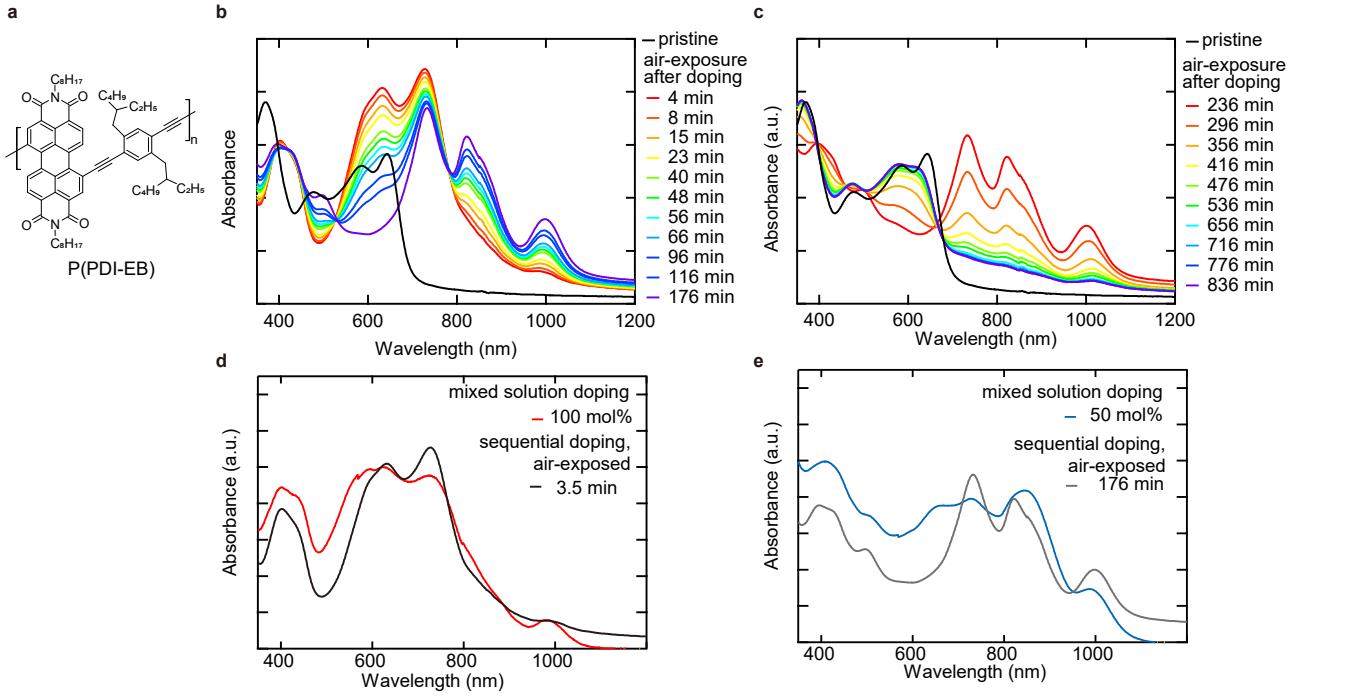

Figure 2 (a) The chemical structure of P(PDI-EB). (b,c) UV-Vis spectra of P(PDI-EB) polymer thin films doped with $(RuCp^*Mes)_2$ by the immersion method. The spectra were measured repeatedly in air without encapsulation. The graph legends show the air-exposure time. The UV-Vis spectrum of a pristine thin film is also shown. (d) Comparison of the absorption spectra of a 100-mol%-doped P(PDI-EB) thin film by mixed solution doping and a thin film doped through immersion after air exposure for 4 min. (e) Comparison of the absorption spectra of a 50-mol%-doped P(PDI-EB) thin film by mixed solution doping and a thin film doped by immersion after air exposure for 176 min.

observed after $(RuCp^*Mes)_2$ doping of a P(PDI-EB) thin film (Figure 2b), which are attributed to the more heavily doped state. Air exposure for 176 min resulted in the observation of peaks at 733, 822, and 1000 nm (Figure 2b), which characterise the less heavily doped state. Further air exposure resulted in recovery to the neutral state, where the pristine thin film without doping showed peaks at 586 and 643 nm (Figure 2c). Very similar absorption strength of the observed peaks in dedoped and pristine thin films in the range of 350–700 nm suggests that the dedoping process converts the n-doped polymer dominantly to the original neutral polymer without chemical deformation. The more heavily doped state was also observed when P(PDI-EB) was doped with $CoCp_2$, where the doped film immediately dedoped to a neutral state, likely owing to the instability of $CoCp_2$. (Supplementary Figure S3†). Similar to the results for the P(NDI2OD-T2) samples, the lifetime of the doped state of P(PDI-EB) was prolonged by two orders of magnitude by using $(RuCp^*Mes)_2$ instead of $CoCp_2$.

The less heavily doped state observed in $(RuCp^*Mes)_2$-doped P(PDI-EB) showed characteristic absorption peaks with maximum intensities at 733, 822, and 1000 nm, which is consistent with the radical anion state of perylene diimide species[29]. Observation of radical anion state is expected to appear when the 50 mol% of $(RuCp^*Mes)_2$ dopant added to the polymer undergoes cleavage and charge-transfer reactions, which was verified by employing mixed-solution doping in our study. UV-Vis absorption spectra of a thin film drop-cast from a mixed solution containing both P(PDI-EB) and 50 mol% $(RuCp^*Mes)_2$ (i.e. potentially able to contribute 1 electron per monomer after cleavage) were consistent with the less heavily doped state observed in sequential doping (Figure 2e). Small differences in the absorption spectra of samples prepared by mixed-solution and sequential doping were observed, which is likely due to morphological differences. These results show that the less heavily doped state corresponds to the P(PDI-EB) with each PDI unit reduced to its radical anion.

The peak positions in the absorption spectrum of the more heavily doped state were blue-shifted compared to that of the less heavily doped state, which is consistent with the changes from radical anions to dianions observed in PDI small molecules[29]. The more heavily doped state was generated by mixed-solution doping with 100 mol% of $(RuCp^*Mes)_2$ where the introduced dopants were potentially able to contribute 2 electrons per monomer (Figure 2d). This result suggests a possibility that the observed more heavily doped state corresponds to the dianion state of the P(PDI-EB).

The doped states were further examined by Fourier-transform infrared spectroscopy (FTIR). Thin films were fabricated on glass substrates by drop-casting mixed solutions of P(PDI-EB) and $(RuCp^*Mes)_2$. The spectra were measured from the front side of thin-films in attenuated total reflection (ATR) mode in air. The intensity of the spectra was normalised based on the peak area of the 2800–3000 cm^{-1} region. These peaks originated from the vibrational modes of aliphatic chains present mainly in the side chains of P(PDI-EB), which are likely to be least affected by doping. To assign vibrational modes of the carbonyl groups, which are often used to quantitatively estimate the doping level[30], these vibrational modes were simulated by density functional theory (DFT) calculations performed on a model small molecule that represents a monomer of P(PDI-EB) in neutral, radical anion, and dianion states. The B3LYP functional, 6-31+G(d) basis set, and reported scaling factors to correct vibrational frequencies[31] were applied. The optimised structures and other details are given in Supplementary Figure S4†.

The FTIR spectrum of the pristine film agreed well with the simulated peak of the neutral model compound in the range of 1400–1800 cm^{-1} (black lines in Figure 3a). The peak labeled v1 is a vibrational mode mainly associated with the conjugated ring, while v2 and v3 are associated with the stretching of carbonyl groups (Supplementary Table 1–3†). Note that each vibrational mode was split into two peaks owing to the structural asymmetry introduced by the diethynylbenzene group in the model compound. Introduction of $(RuCp^*Mes)_2$ up to 50 mol% (i.e. potentially able to contribute 1 electron per monomer) results in the redshift of the v1–v3 peaks, which is consistent with n-doping of P(PDI-EB) leading to the formation of the radical anion state. This suggests that the introduced 50 mol% of dopant quantitatively reduces the neutral polymer into the radical anion state via the formation of a cleaved $RuCp^*Mes^+$, which is consistent with our UV-vis absorption measurements. When the amount of $(RuCp^*Mes)_2$ was increased from 50 mol% up to 100 mol%, the observed peak positions shifted further towards lower wavenumbers, which is consistent with the changes from the radical anion to the dianion state in our calculations. With the exception of the v3 peak, although the observed peaks overlap with each other around 1520–1600 cm^{-1}, the observed spectra did not contradict the simulated dianion state. Overall, UV-vis-NIR, FTIR, and DFT calculations suggest the formation of dianion states of P(PDI-EB) when doped with $(RuCp^*Mes)_2$. A previous study proposed that 6,13-bis(triisopropylsilylethynyl)pentacene is doped into a dianion in solution through a redox reaction with a dimerized metallocene[32], our findings suggests that doping of P(PDI-EB) with $(RuCp^*Mes)_2$ up to the dianion state is feasible, even in a solid-state thin film.

The ionization potentials (*IP*s) of pristine and $(RuCp^*Mes)_2$-doped thin films were determined using photoelectron yield spectroscopy (PYS) measurements, which gives us insight into energetics of doping. The immersion method was used for both P(NDI2OD-T2) and P(PDI-EB) polymer films fabricated on ITO-coated glass substrates. Thin-film samples were placed into a vacuum chamber to measure the threshold energy giving rise to a photoelectron current, which corresponds to *IP*. Note that the work function is equal to or less than the *IP* of the doped films evaluated in our experiments.

The *IP* of pristine polymeric semiconductor films is at the edge of the density of states originating from the highest occupied molecular orbital (HOMO). In our study, the pristine P(NDI2OD-T2) and P(PDI-EB) films showed large *IP* (Figure 4a), which agrees with the deep HOMO levels expected for electron-transporting materials; the obtained values are similar to those previously reported from UV photoelelectron spectroscopy (5.5 eV[33] for P(NDI2OD-T2) and 6.1 eV[23] for P(PDI-EB)). The thin films doped with $(RuCp^*Mes)_2$ by the immersion method showed large shifts in *IP* owing to the filling of their empty density of states through chemical doping

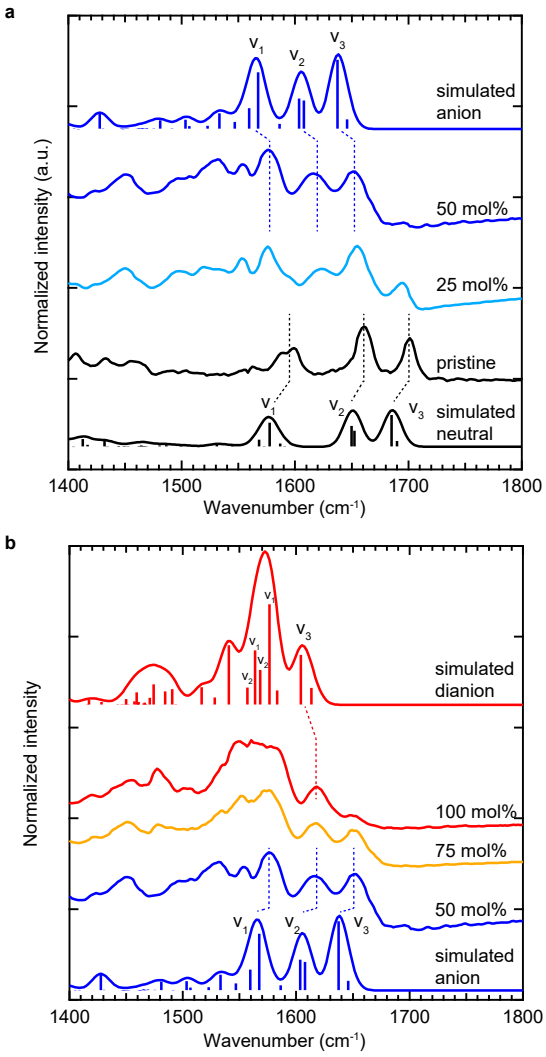

Figure 3 (a) FTIR spectra of a pristine and 50-mol%-doped P(PDI-EB) thin films by mixed-solution doping. Simulated spectra for pristine and radical anion monomers are also presented. (b) FTIR spectra of 50-mol%- and 100-mol%-doped P(PDI-EB) thin films. Simulated spectra for a radical anion and a dianion monomer are also presented.

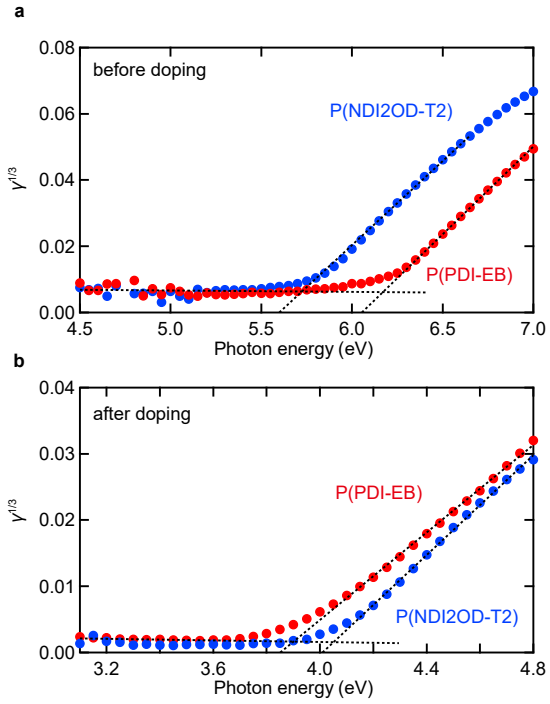

Figure 4 (a) PYS spectra of pristine polymeric semiconductor thin films measured with a deuterium lamp. (b) PYS spectra of the doped polymeric semiconductor thin films measured with a xenon lamp. The immersion method with $(RuCp^*Mes)_2$ was employed for chemical doping.

Table 1 Electronic properties of $(RuCp^*Mes)_2$-doped polymer thin films prepared using the immersion method, which were exposed to air for a short time before measurements. The air exposure time was 5 min for conductivity measurements.

	σ (S cm^{-1})	*IP* (eV) pristine	*IP* (eV) doped
P(NDI2OD-T2)	1.2×10^{-5}	5.72	4.15
P(PDI-EB)	4.5×10^{-5}	6.16	3.90

(Figure 4b). Based on our UV-Vis study with $(RuCp^*Mes)_2$ immersion doping, the P(NDI2OD-T2) thin film was in its less heavily doped state while the P(PDI-EB) thin film was in its more heavily doped state. Considering the observed shallow *IP*s, charge transfer reaction with oxygen in air is anticipated for the $(RuCp^*Mes)_2$-doped polymers [10], which is likely the main cause of dedoping observed in UV-vis measurements. In our PYS measurements, the doped P(NDI2OD-T2) and P(PDI-EB) thin films were exposed to air for a short time to move them into the measurement chamber. Conductivity σ of doped P(NDI2OD-T2) and P(PDI-EB) thin films after air exposure for 5 min is summarized in Table 1, where the measurement was conducted in an Ar atmosphere.

Finally, we show that control over the initial doping level is feasible in our immersion method. Similar to the standard immersion method, a polymeric semiconductor film on a glass substrate was immersed in pure *n*BA kept in a vial. While heating the vial, diluted $(RuCp^*Mes)_2$ solution (0.05 mM) was added to the vial with a micropipette. Here, 10 μL of solution containing 0.5 nmol of $(RuCp^*Mes)_2$ was added repeatedly to the system, which was a sufficiently small amount to tune the extent of doping of a polymer semiconductor thin film. Indeed, a P(PDI-EB) thin film doped using this method showed conductivity dependent on the amount of added dopant solution (Figure 5). Compared to a thin film without doping (2×10^{-7} S cm^{-1}), doped films show higher conductivity values. After the initial increase of the conductivity with the introduced amount of dopant, the conductivity decreases with the increasing amount of dopant, which is consistent with reported doping level dependence of conductivity for n-type polymeric semiconductors [15,34]. This method could help tune the amount of doping and electronic properties of electron-transporting molecule semiconductors.

Conclusion

We have demonstrated strong, stable, and controllable n-type sequential doping of polymeric semiconductors with $(RuCp^*Mes)_2$.

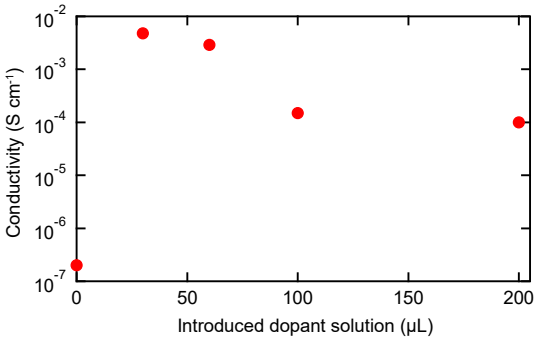

Figure 5 Conductivity of P(PDI-EB) thin films doped through the modified immersion method. Varying amounts of 0.05 mM $(RuCp^*Mes)_2$ solution were introduced to the system at 80 °C to control the doping level.

A high cathodic reduction potential for $RuCp^*Mes^+$ inhibits the back-charge transfer process, which results in moderate ambient stability of the doped polymers. This is in contrast to doping with $CoCp_2$, where charged and neutral states coexist in a chemical equilibrium, providing pathways for decomposition via neutral dopant species in ambient air. The vastly different dedoping kinetics resulted in the $(RuCp^*Mes)_2$-doped samples showing a timescale of dedoping over two orders of magnitude longer than that of $CoCp_2$-doped samples. Although the generation of a heavily doped state has been previously reported only in electrochemical studies with high applied biases, here we observed that sequential doping with $(RuCp^*Mes)_2$ was able to generate this state in P(NDI2OD-T2) thin films. Furthermore, the heavily doped state observed in $(RuCp^*Mes)_2$-doped P(PDI-EB) is thought to be the dianion state of this polymer. Photoelectron measurements show that ionization potentials of the polymers considerably decrease upon $(RuCp^*Mes)_2$ doping owing to filling of empty density of states. These attractive features reduce the limitations of processing and handling of n-doped materials. We anticipate that our findings will promote the development of other dopant-semiconductor combinations for increasingly air-stable doped materials.

Experimental

P(NDI2OD-T2) was purchased from Ossila. P(PDI-EB) (Mw ∼ 45,000 Da and PDI ∼ 3.30)[23] and $(RuCp^*Mes)_2$[35] were synthesized as described elsewhere. Glass substrates were used for UV-Vis and FTIR measurements. For PYS measurements, ITO-coated glass substrates were used. For conductivity measurements, glass substrates with thermally deposited Cr/Au contacts were used, where the sample geometry was in a in-plane, 2-terminal configuration with a channel length of 200 μm and width of 2 mm.

All film-fabrication processes were performed in protective N_2 or Ar atmospheres. For sequential doping, the thin films were fabricated from 0.6 wt% polymer solutions in chloroform by spin-coating at 3000 rpm. The films were then dried at 120 °C for 5 min and annealed at 200 °C for 30 min. The thickness of the films was 70 ±5 nm, as measured with an atomic force microscope. In the immersion method, the thin films were placed in a small vial with 1 mL of *n*BA. While heating the system at 80 °C, 30–40 μL of 2 mM dopant solution in *n*BA was added to the vial. In the drop-casting method, the dopant solution was drop-casted onto thin films at 80 °C. For the encapsulation of $CoCp_2$-doped thin films, the top surface of the doped film was covered with CTL-809M and a glass substrate to sandwich the thin film between two glass substrates.

In the mixed-solution doping for FTIR and UV-Vis studies, *o*-dichlorobenzene solutions with 2.6 mM of P(PDI-EB) and varying amounts of $(RuCp^*Mes)_2$ with the specified molar ratio were prepared. The thin films were fabricated by drop-casting on a 100 °C hot plate followed by annealing at 130 °C for 45 min. The absorption spectra of the thin films fabricated using the mixed-solution method were encapsulated by sandwiching the film with glass substrates sealed at the edges using vacuum grease.

Absorption spectra were obtained in air using a V-670 (JASCO) instrument. The electrical conductivity of the samples was measured using an Agilent E5270B system in an Ar atmosphere. PYS measurements were conducted with a SUMITOMO PYS-202 system under vacuum using a turbomolecular pump system, where a deuterium lamp or xenon lamp were used to characterise the pristine or doped films, respectively.

Conflicts of interest

There are no conflicts to declare.

Acknowledgments

Y.Y. acknowledges support from Materials Education program for the future leaders in Research, Industry, and Technology (MERIT), and from JSPS. S. J. thanks the United States-India Educational Foundation (USIEF, India) and Institute of International Education (IIE, USA) for a Fulbright-Nehru Postdoctoral Fellowship (Grant No. 2266/FNPDR/2017). D.B. acknowledges financial support from Indo US Science & Technology Forum (IUSSTF), DST Government of India. S.W. acknowledges support from PRESTO-JST through the project “Hyper-nanospace Design Toward Innovative Functionality" (Grant no. JPMJPR151E), and from the Leading Initiative for Excellent Young Researchers of JSPS. This work was also supported in part by JSPS KAKENHI grants (nos. 16J07912 and JP20K15358). Work at Georgia Tech was supported by the National Science Foundation (through DMR-1807797 and the DMREF program DMR-1729737).

Notes and references

1 I. E. Jacobs and A. J. Moulé, *Advanced Materials*, 2017, **29**, 1703063.
2 B. Lüssem, M. Riede and K. Leo, *Physica Status Solidi A*, 2013, **210**, 9–43.
3 J.-K. Tan, R.-Q. Png, C. Zhao and P. K. Ho, *Nature Communications*, 2018, **9**, 1–8.
4 W.-L. Seah, C. G. Tang, R.-Q. Png, V. Keerthi, C. Zhao, H. Guo, J.-G. Yang, M. Zhou, P. K. Ho and L.-L. Chua, *Advanced Functional Materials*, 2017, **27**, 1606291.
5 Y. Kim, S. Chung, K. Cho, D. Harkin, W.-T. Hwang, D. Yoo, J.-K. Kim, W. Lee, Y. Song, H. Ahn *et al.*, *Advanced Materials*, 2019, **31**, 1806697.
6 I. E. Jacobs, E. W. Aasen, J. L. Oliveira, T. N. Fonseca, J. D. Roehling, J. Li, G. Zhang, M. P. Augustine, M. Mascal and A. J. Moulé, *Journal of Materials Chemistry C*, 2016, **4**, 3454–3466.
7 K. Kang, S. Watanabe, K. Broch, A. Sepe, A. Brown, I. Nasrallah, M. Nikolka, Z. Fei, M. Heeney, D. Matsumoto *et al.*, *Nature Materials*, 2016, **15**, 896–902.
8 R. Fujimoto, Y. Yamashita, S. Kumagai, J. Tsurumi, A. Hinderhofer, K. Broch, F. Schreiber, S. Watanabe and J. Takeya, *Journal of Materials Chemistry C*, 2017, **5**, 12023–12030.
9 Y. Yamashita, J. Tsurumi, M. Ohno, R. Fujimoto, S. Kumagai, T. Kurosawa, T. Okamoto, J. Takeya and S. Watanabe, *Nature*, 2019, **572**, 634–638.
10 C. G. Tang, M. C. Ang, K.-K. Choo, V. Keerthi, J.-K. Tan, M. N. Syafiqah, T. Kugler, J. H. Burroughes, R.-Q. Png, L.-L. Chua *et al.*, *Nature*, 2016, **539**, 536.
11 X. Zhan, Z. Tan, B. Domercq, Z. An, X. Zhang, S. Barlow, Y. Li, D. Zhu, B. Kippelen

and S. R. Marder, *Journal of the American Chemical Society*, 2007, **129**, 7246–7247.
12 H. Yan, Z. Chen, Y. Zheng, C. Newman, J. R. Quinn, F. Dötz, M. Kastler and A. Facchetti, *Nature*, 2009, **457**, 679–686.
13 J. E. Anthony, A. Facchetti, M. Heeney, S. R. Marder and X. Zhan, *Advanced Materials*, 2010, **22**, 3876–3892.
14 H. Fu, Z. Wang and Y. Sun, *Angewandte Chemie International Edition*, 2019, **58**, 4442–4453.
15 E. E. Perry, C.-Y. Chiu, K. Moudgil, R. A. Schlitz, C. J. Takacs, K. A. O'Hara, J. G. Labram, A. M. Glaudell, J. B. Sherman, S. Barlow *et al.*, *Chemistry of Materials*, 2017, **29**, 9742–9750.
16 B. D. Naab, X. Gu, T. Kurosawa, J. W. To, A. Salleo and Z. Bao, *Advanced Electronic Materials*, 2016, **2**, 1600004.
17 X. Zhao, D. Madan, Y. Cheng, J. Zhou, H. Li, S. M. Thon, A. E. Bragg, M. E. DeCoster, P. E. Hopkins and H. E. Katz, *Advanced Materials*, 2017, **29**, 1606928.
18 C.-Y. Yang, Y.-F. Ding, D. Huang, J. Wang, Z.-F. Yao, C.-X. Huang, Y. Lu, H.-I. Un, F.-D. Zhuang, J.-H. Dou *et al.*, *Nature Communications*, 2020, **11**, 1–10.
19 A. F. Paterson, A. Savva, S. Wustoni, L. Tsetseris, B. D. Paulsen, H. Faber, A. H. Emwas, X. Chen, G. Nikiforidis, T. C. Hidalgo *et al.*, *Nature Communications*, 2020, **11**, 1–11.
20 N. G. Connelly and W. E. Geiger, *Chemical Reviews*, 1996, **96**, 877–910.
21 S. Guo, S. B. Kim, S. K. Mohapatra, Y. Qi, T. Sajoto, A. Kahn, S. R. Marder and S. Barlow, *Advanced Materials*, 2012, **24**, 699–703.
22 X. Lin, B. Wegner, K. M. Lee, M. A. Fusella, F. Zhang, K. Moudgil, B. P. Rand, S. Barlow, S. R. Marder, N. Koch *et al.*, *Nature Materials*, 2017, **16**, 1209–1215.
23 S. G. Hahm, Y. Rho, J. Jung, S. H. Kim, T. Sajoto, F. S. Kim, S. Barlow, C. E. Park, S. A. Jenekhe, S. R. Marder *et al.*, *Advanced Functional Materials*, 2013, **23**, 2060–2071.
24 O. V. Gusev, M. A. Ievlev, M. G. Peterleitner, S. M. Peregudova, L. I. Denisovich, P. V. Petrovskii and N. A. Ustynyuk, *Journal of Organometallic Chemistry*, 1997, **534**, 57–66.
25 A. Rajagopal and A. Kahn, *Journal of Applied Physics*, 1998, **84**, 355–358.
26 D. Trefz, A. Ruff, R. Tkachov, M. Wieland, M. Goll, A. Kiriy and S. Ludwigs, *The Journal of Physical Chemistry C*, 2015, **119**, 22760–22771.
27 R. Brandon, J. Osiecki and A. Ottenberg, *The Journal of Organic Chemistry*, 1966, **31**, 1214–1217.
28 S. K. Mohapatra, A. Fonari, C. Risko, K. Yesudas, K. Moudgil, J. H. Delcamp, T. V. Timofeeva, J.-L. Brédas, S. R. Marder and S. Barlow, *Chemistry–A European Journal*, 2014, **20**, 15385–15394.
29 R. O. Marcon and S. Brochsztain, *The Journal of Physical Chemistry A*, 2009, **113**, 1747–1752.
30 S. Seifert, D. Schmidt and F. Würthner, *Chemical Science*, 2015, **6**, 1663–1667.
31 J. P. Merrick, D. Moran and L. Radom, *The Journal of Physical Chemistry A*, 2007, **111**, 11683–11700.
32 S. Guo, S. K. Mohapatra, A. Romanov, T. V. Timofeeva, K. I. Hardcastle, K. Yesudas, C. Risko, J.-L. Brédas, S. R. Marder and S. Barlow, *Chemistry–A European Journal*, 2012, **18**, 14760–14772.
33 Y. Qi, S. K. Mohapatra, S. Bok Kim, S. Barlow, S. R. Marder and A. Kahn, *Applied Physics Letters*, 2012, **100**, 54.
34 K. Shi, F. Zhang, C.-A. Di, T.-W. Yan, Y. Zou, X. Zhou, D. Zhu, J.-Y. Wang and J. Pei, *Journal of the American Chemical Society*, 2015, **137**, 6979–6982.
35 H.-I. Un, S. A. Gregory, S. K. Mohapatra, M. Xiong, E. Longhi, Y. Lu, S. Rigin, S. Jhulki, C.-Y. Yang, T. V. Timofeeva *et al.*, *Advanced Energy Materials*, 2019, **9**, 1900817.